Proceedings of the 28th IEEE
EMBS Annual International Conference
New York City, USA, Aug 30-Sept 3, 2006

Femoral Fracture Risk Assessment after Intensity Modulated Radiation Therapy (IMRT) for the Treatment of Soft Tissue Sarcoma Using a Novel Mathematical Model

Yan Song, Song Wang, Maria Chan, Burman Chandra,
Atam Dhawan, *Fellow*, *IEEE*, and Yulin Song, *Member*, *IEEE*

***Abstract*---Intensity modulated radiation therapy (IMRT) is often used for the treatment of soft tissue sarcoma. Due to high radiation doses, many patients have high risk of suffering from a femoral bone fracture sometime following the IMRT treatment. The most common type of radiation treatment-related fracture is a stress fracture. The fracture risk rate may be as high as 24% in sarcoma patients who have undergone periosteal stripping and received chemotherapy. Thus, it is necessary to be able to identify those patients with high risk for IMRT treatment-related bone fracture. In this paper, we will first present IMRT treatment planning techniques. We will then discuss how bone system changes their stiffness and how the fracture risk develops after a certain period of time post radiation treatment. Finally, we will present our latest data on the femoral bone fracture risk factor assessment for patients with soft tissue sarcoma following IMRT treatment. We have developed a novel mathematical model of trabecular bone composed of a disordered cubic network. Based on our preliminary data, we believe that this new mathematical model could shed new light on the relationship between the femoral bone fracture risk factor and the radiation dose delivered by an IMRT plan and provide a valuable prognostic tool for these high-risk patients.**

I. INTRODUCTION

Currently, intensity modulated radiation therapy (IMRT) is often employed as an adjuvant treatment in conjunction with surgical resection for the treatment of soft tissue sarcoma. Recent studies have indicated that wide excision followed by irradiation has resulted in excellent local control. Since many tumors are in close proximity to bone, it is therefore necessary to perform excision of periosteum to obtain a clear margin. However, periosteal stripping unavoidably disrupts the nutrient vessels to bone and compromises the vasculature of the outer cortex. In addition, high radiation doses delivered to long bones by IMRT plans also affect bones in many aspects. Hematopoietic cells of bone marrow are extremely sensitive to radiation. Studies have shown that radiation dose at the level of ~ 1 Gy can produce bone marrow suppression. Lethal or sublethal damage to stem cells incurred by radiotherapy prevents them from developing into differentiated myeloid and lymphocytic cells. In addition, osteoblasts and mesenchymal stem cells also are radio-sensitive. Irradiation can reduce metabolic bone formative activity. It has been reported that as low as 8 Gy can inhibit the formation of heterotopic ossification.

The most common type of radiation treatment-related bone fracture is a stress fracture. The fracture risk rate may be as high as 24 % in sarcoma patients who have undergone periosteal stripping and received chemotherapy. Thus, it is necessary to be able to identify those patients with high risk for IMRT treatment-related fracture. Since all sarcoma patients will have a follow-up CT scan upon completion of IMRT treatments. It would be very meaningful to develop a technique to assess the femoral fracture risk based on CT data. In this study, a novel mathematical model of trabecular bone composed of a disordered cubic network was employed to assess the femoral fracture risk factor for patients after IMRT treatment. The post-IMRT treatment fracture risk factor will be compared with that of the pre-IMRT treatment. In this paper, we will first present IMRT technique. We will then discuss our mathematical model based on a cubic lattice spring array and illustrate how to model a bone response under external loading. Lastly, we will present our data on a femoral bone system and the fracture risk factor computed based on the fracture stress applied on the network system.

II. MATERIALS and METHODS

A. Intensity Modulated Radiation Therapy (IMRT)

Since 2000, IMRT has emerged as the most important radiotherapy modality for cancer treatment. Like conventional radiotherapy techniques, IMRT also

Yan Song is with the Department of Physics, University of Houston, Houston, TX 77024 USA (e-mail: yxs4406@sbcglobal.net).

Song Wang is with the Department of Electrical and Computer Engineering, New Jersey Institute of Technology, Newark, NJ 07102 USA (e-mail: sw29@njit.edu)

Maria Chan is with the Department of Medical Physics, Memorial Sloan-Kettering Cancer Center, New York, NY 10021 USA (e-mail: chanm@mskcc.org).

Chandra Burman is with the Department of Medical Physics, Memorial Sloan-Kettering Cancer Center, New York, NY 10021 USA (e-mail: burmanc@mskcc.org).

Atam Dhawan is with the Department of Electrical and Computer Engineering, New Jersey Institute of Technology, Newark, NJ 07102 USA (e-mail: dhawan@ADM.NJIT.EDU).

Yulin Song is with the Department of Medical Physics, Memorial Sloan-Kettering Cancer Center, New York, NY 10021 USA (corresponding author, phone: 973-983-7311; fax: 973-983-7301; e-mail: songy@mskcc.org).

employs the use of ionizing radiation for cancer treatment to control and destroy malignant cells. IMRT treatment planning process consists of patient simulation, CT scan, target volume delineation, plan optimization, multi-leaf collimator (MLC) leaf sequence generation, and final dose computation [1, 2]. The patient is first simulated on a simulator to determine the iso-center position and the possible treatment beam angles. In theory, the iso-center should be positioned at the geometric center of the target. Once the simulation is completed, the patient is CT scanned in the same position as in the simulation in a customized thermoplastic mold to minimize patient movement during the imaging procedure. At our cancer center, CT images of 2.5 mm slice thickness are acquired over the entire treatment region for treatment planning purpose. The planning target volume (PTV) is delineated on the CT images by the radiation oncologist. The PTV is created by adding certain amount of margin around the gross tumor volume (GTV) to account for target uncertainty caused by patient treatment setup error. To achieve a better target dose coverage, a new structure named PTV_X is created by extending PTV superiorly and inferiorly one slice. In addition, a tuning structure, RIND, is generated by expanding PTV_X by 2 cm axially to fine tune the dose distribution. The treatment planner delineates the involved femur because it is the organ at risk in this setting and needs to be spared.

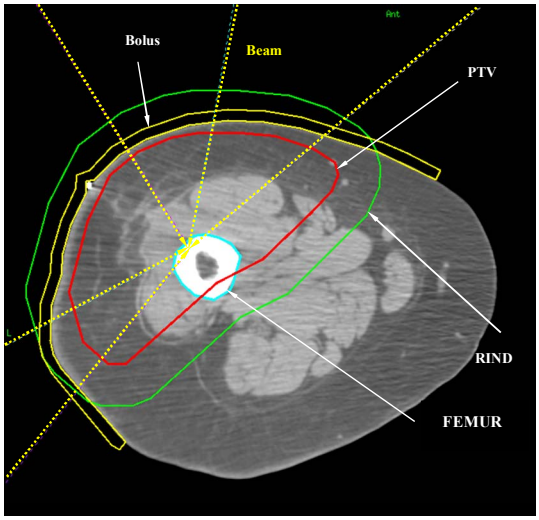

Figure 1. Structure definitions and beam angle arrangement. In this particular case, the tumor was in the left leg.

Based on our clinical experience, a four or five beam plan is necessary to create a concave dose distribution around the femur. In selecting beam angles, all the beams enter the target from one side of the leg to spare a longitudinal strip of soft tissue. In addition, efforts are made to ensure that no beams entering or exiting through the uninvolved leg. Furthermore, all beams should not pass through or be close to genital organs for patients with a tumor in the upper thigh and pelvic region. The collimator of each beam should be rotated to conform to the contour of the PTV for the best beam shaping.

Figure 1 shows the volume definitions and beam angle arrangement for a representative soft tissue sarcoma IMRT plan. In this particular case, the tissue equivalent bolus material was used to boost the dose to the skin as the tumor was very superficial. In this study, the IMRT plans were computed using an MSKCC in-house treatment planning system. Given a set of dose constraints, each IMRT plan was optimized based on a quadratic objective function. Once optimal beam intensity profiles or maps were obtained, MLC leaf sequences were generated using the dynamic MLC (DMLC) technique. Based on these leaf sequences, the final dose distribution was then computed using a pencil beam algorithm. If the criteria for plan acceptance were not met, a trade-off between the target dose coverage and constraints would have to be made. The patients were treated with 6 MV photons on a Varian Clinac 21EX (Palo Alto, CA) equipped with a 120-leaf MLC. Figure 2 shows the MLC aperture projected on the digitally reconstructed radiograph (DRR) at a beam angle of 50^0.

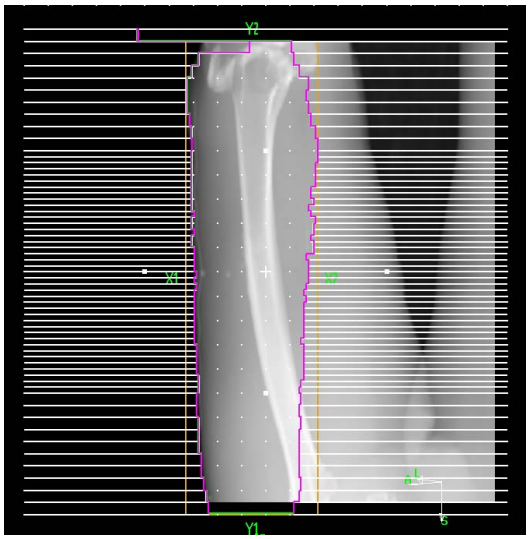

Figure 2. A representative MLC aperture at a beam angle of 50^0. In this particular case, the entire thigh was treated because the enormous size of the tumor. The open area was part of the leg that needed to be treated. The other areas were blocked by the MLC.

B. Spring-Lattice Model

In order to quantitatively estimate the effects of IMRT treatments on human skeleton system, a mathematical spring-lattice model [4] was used. In this model, a bone specimen is replaced by a system of springs where each occupied voxel (i.e., cubic volume element) is represented by a set of linear elastic elements as described below [5, 6]. The choices of springs and their elastic moduli are set

by the following requirement: a spring network that is constructed to represent an isotropic region should itself be isotropic [5, 6]. Although it is known that no cubic-type network can satisfy this condition exactly [6], the following combination was shown to provide a stable and approximately isotropic configuration of elastic elements. Each occupied cubic voxel is replaced by a set of 24 elements; 12 of these with identical elastic constant k lie along the sides of the cube, while the remaining 12, with elastic moduli $2k$, are placed along the face-diagonals [5]. Mechanical properties of each bone specimen are studied using the corresponding "lattice-spring network" constructed by replacing each occupied voxel by such a combination of springs.

Each network is subjected to vertical compression with the following boundary conditions. Nodes on the lower surface are free to move horizontally, but their vertical locations are unchanged. Those on the upper surface are compressed vertically by ς and are free to move horizontally. All those remaining nodes are constrained only by elastic elements connecting them to neighbors. The elastic potential energy of the compressed network can be calculated from the ordinates of the nodes, which are the independent variables in the system. Equilibrium of the network subjected to a compression ς is calculated by minimizing its elastic energy using the conjugate gradient method [7].

In order to calculate the fracture load of a network, we require a condition on the failure of individual elements. Several recent experiments have demonstrated that fracture strains for specimens of human trabecular bone of a fixed size from specific anatomical locations are nearly constant for a wide range in age, even though the corresponding fracture load can vary by more than an order of magnitude [8, 9, 10, 11, 12]. We assume a corresponding fixed-fracture-strain condition for each voxel. Thus, we do not model consequences of age-related changes in material properties of bone tissue, such as can be expected with increased levels of mineralization. The effects of such changes (when available experimentally) are easily included since the fracture load of our models is linearly related to the fracture strain [13].

Specifically, we model the failure of bone tissue with a strain-based criterion of individual voxels, i.e., at each value of ς: those voxels that are strained beyond a pre-set value η are removed from the model network. The amount of strain used in these considerations is the eigenvalue of the strain tensor with largest magnitude [6]. Thus, the failure of a voxel is associated with it being strained beyond η (in tension or compression) along any one direction. Under this scenario, we find that failure strains of lattice-spring networks remain nearly fixed during degradation. It should be noted that the fracture strain of a bone specimen is expected to reduce with increasing size due to the likelihood of larger fractures [13, 14, 15]. In addition, computations show that model specimens exhibit significant plasticity, even though the individual voxels are assumed to be brittle. This is because of the formation of new stress pathways when an existing one is broken [16].

The lattice-spring system needs to be extended in order to model dynamical properties of bone samples. We replace the mass m of material contained within each voxel by identical point masses 1/8 of m placed on each of its eight vertices. Thus, we model mechanical properties of the bone specimen by a network of elastic elements with masses placed on the nodes. The mass m at node i is $n_i^{/}$ m/8, where $n_i^{/}$ is the number of occupied voxels surrounding it. Similarly, the elastic modulus kg_{ij} joining nodes i and j depends on the number of occupied voxels with ij as an edge. The Hamiltonian of the network is

$$H = \sum \frac{p_i^2}{2m_i} + \frac{k}{4} \sum g_{ij}[(u_i - u_j).\hat{x}_{ij}]^2 \qquad (1)$$

where p_i denotes the momentum of the mass at node i and u_i denotes its displacement, $\hat{x}_{ij}$ denotes the unit vector in the direction from node i to node j.

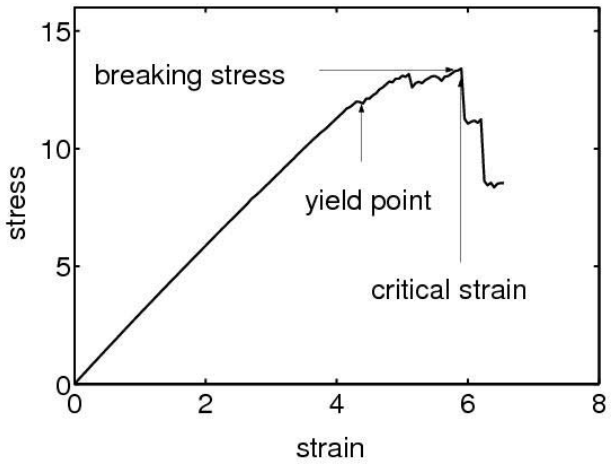

Figure 3. Output stress vs external loading. With uniform increment of compression, stress increases accordingly till the system collapses and stress drops sharply.

To assess the femoral fracture risk, the CT images of the involved femoral bone were converted from the DICOM format to an ASCII file with 512x512x10 array. The physical quantity of each voxel was the CT number, which was linear proportional to the density of that voxel. The elastic constant k was related to each voxel's CT

number. The occupied voxels were replaced by an elastic element (a 24 linear spring system), others were set to zero. When an external mechanical load was applied (indicated by top surface uniform displacement of 0.1), the voxels on the bottom surface were horizontally displaced only. Other voxels adjusted till the energy in Equation 1 reached the minimum. We calculated the relative displacement of the top two layers and obtained the response "force" of the system. If there were some voxels that had bigger strains than our criteria η, this element would be eliminated in our array. Other voxels were affected accordingly and till the avalanche occurred. The response "force" in this case would drop sharply as indicated in Figure 3. In the bone system shown in Figure 1, the bone array was structurally uniform and each voxel bore the loading with equal weight. Avalanche would never happen and bulk distribution of strain was uniform. The response linearly increased with the external loading in a large range of value.

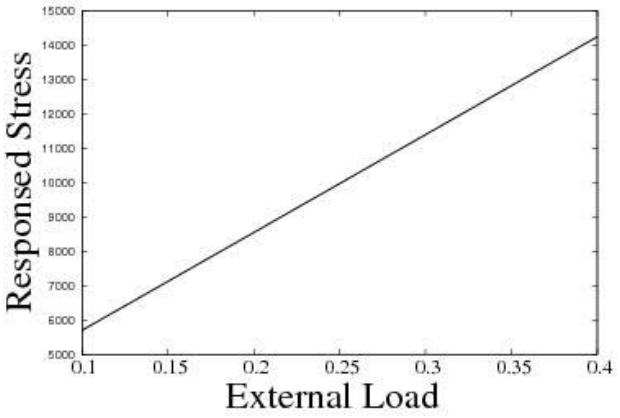

Figure 4. The mechanical response under increasing loading for a soft tissue sarcoma case prior to IMRT treatments (Arbitrary unit).

III. CONCLUSION

In this preliminary study, we emphasized the significance of soft tissue sarcoma treatment using IMRT. Our particular interests were focused on how IMRT treatments affected the healthy bone system and the development of a mathematical model for predicting the femoral fracture risk. It is expected that the spring-lattice model is a very useful and valuable tool in dealing with the mechanical stimuli of bone systems. This model can be applied to the bone systems that have undergone radiation treatment for soft tissue sarcoma.

As indicated in Figure 4, the mechanical response of the healthy bone was linearly proportional to the applied load (with increment of 0.1 of the top layer displacement). The units shown in Figure 4 were arbitrary. Since there was no perforation, the stress was uniformly distributed in the bulk of bone, so fracture did not appear. The slope in Figure 4 indicates the stiffness of the bone and can be regarded as a characteristic of the bone system. Once we have the CT data after the IMRT treatment, we can compute this slope and thus, determine how IMRT affects the bone stiffness. Currently, we are waiting for the post-IMRT treatment CT data. By comparing the slope difference of the pre- and post-IMRT loading-response curves, we will be able to tell the effects of IMRT treatments on the femoral bone strength and its fracture risk. Considering the increasing number of soft tissue sarcoma patients will receive IMRT treatments, the potential applications of this model in radiation oncology need to be fully explored and investigated.

REFERENCE

[1] L. Xing, Q. Wu, Y. Yang, and A. Boyer, "Physics of IMRT", In: Intensity Modulated Radiation Therapy – A Clinical Perspective. BC Decker, Lewiston, NY, 2004.

[2] Y. Song, A. Boyer, Pawlicki T, *et al.* Modulated electron radiation therapy-emerging technology. In: Intensity Modulated Radiation Therapy – A Clinical Perspective. BC Decker, Lewiston, NY, 2004.

[3] G.H. Gunaratne, K.K. Mohanty, and S.J. Wimalawansa, *Phys. A*, vol. 315, p.98, 2002.

[4] G. H. Gunaratne, C. S. Rajapaska, K. E. Bassler, K. K. Mohanty, and S.J. Wimalawansa, *Phys.Rev.Lett.* **88** 068101, 2002

[5] A. J. C. Ladd, J. H. Kinney, and T. M. Breunig, "Deformation and Failure of Cellular Material," *Phys. Rev. E*, **55**, p.3271, 1997.

[6] A. J. C. Ladd and J. H. Kinney, "Elastic Constant of Cellular Structures," *Physica A*, **240**, p.349-360, 1997.

[7] W. H. Press, B. P. Flannery, S. A. Teukolsky, and W. T. Vettering, *Numerical Recipes-The Art of Scientific Computing,* (Cambridge University Press, Cambridge, 1988.

[8] T. E. Ciarelli, D.P. Fyhrie, M.B. Schaffler, and S.A. Goldstein, "Variations in Three-dimensional Cancellous Bone Architecture of the Proximal Femur in Female Hip Fractures and in Controls," *J. Bone Miner. Res*., **15(1)**, p.32-40, 2000.

[9] E. F. Morgan, H. H. Bayraktar, O. C. Yeh, S. Majumdar, A. Burghardt, and T. M. Keaveny, "Contribution of Inter-site Variations in Architecture to Trabecular Bone Apparent-Yield Strains," *J. Biomech.*, **37**, p.1413-1420, 2004.

[10] E. F. Morgan and T. M. Keaveny, "Dependence of Yield Strain of Human Trabecular Bone on Anatomic Site," *J. Biomech.*, **34**, p.569-577, 2001.

[11] S. D. Ryan and J. L. Williams, "Tensile Testing of Rodlike Trabecule Excised from Bovine Femoral Bone," *J. Biomech.*, **22**, p.351-355, 1989.

[12] J. Y. Rho, R. B. Ashmas, and C. H. Turner, "Young's Modulus of Trabeculae and Cortical Bone Material: Ultrasonic and Microtensile Measurements," *J. Biomech*., **26**, p.111-119, 1993 **.**

[13] C.S. Rajapakse, J. S. Thomsen, J. S. Espinoza-Ortiz, S. J. Wimalawansa, E. N. Ebbesen, Li Mosekilde, and G. H. Gunaratne, "An Expression Relating Breaking Stress and Density of Trabecular Bone," *J. Biomech*., **37**, p.1241-1249, 2004.

[14] D. G. Harlow, and S. L. Phoenix, "Probability Distributions for the Strength of Composite Materials II. A Convergent Sequence of Tight Bounds," *Intl. J. Fracture*, **17**, p.601-630, 1981.

[15] H. Gao, B. Ji, I. L. J $\ddot{a}$ ger, E. Artz, and P. Fratzl, "Materials Become Insensitive to Flaws at Nanoscale: Lessons from Nature," *Proc. Natl. Acad. Sci. USA*, **100**, p.5597-5600, 2003.

[16] M. A. K. Liebschner, R. M $\ddot{u}$ ller, C. S. Rajapakee, S. J. Wimalawansa, and G. H. Gunaratne, "Testing Two-predictions for Fracture Load Using Computer Models of Trabecular Bone," *Biophys. J*. **89**, p.759-767, 2005.